Modeling of micro-grinding forces considering dressing parameters and tool deflection

(article starts on next page)

Modeling of micro-grinding forces considering dressing parameters and tool deflection

Mohammadali Kadivar [a,b,*], Bahman Azarhoushang [a], Peter Krajnik [b]

[a] Institute of Precision Machining (KSF), Furtwangen University of Applied Sciences, Jakob-Kienzle-Str 17, 78056, Villingen-Schwenningen, Germany
[b] Department of Industrial and Materials Science, Chalmers University of Technology, Hörsalsvägen 7B, SE-412 96, Gothenburg, Sweden

ARTICLE INFO

ABSTRACT

The prediction of cutting forces is critical for the control and optimization of machining processes. This paper is concerned with developing prediction model for cutting forces in micro-grinding. The approach is based on the probabilistic distribution of undeformed chip thickness. This distribution is a function of the process kinematics, properties of the workpiece, and micro-topography of the grinding tool. A Rayleigh probability density function is used to determine the distribution of the maximum chip thickness as an independent parameter. The prediction model further includes the effect of dressing parameters. The integration of the dressing model enables the prediction of static grain density of the grinding tool at various radial dressing depths. The tool deflection is also considered in order to account for the actual depth of cut in the modeling process. The dynamic cutting-edge density as a function of the static grain density, the local tool deflection, elastic deformation, and process kinematics can hence be calculated. Once the chip thickness is calculated, the single-grain forces for individual abrasive grains are predicted and the specific tangential and normal grinding forces simulated. The simulation results are experimentally validated via cutting-force measurements in micro-grinding of Ti6Al4V. The results show that the model can predict the tangential and normal grinding forces with a mean accuracy of 10% and 30%, respectively. The observed cutting forces further imply that the flow stress of the material did not change with changing the cutting speed and the cutting strain rate. Moreover, it was observed that the depth of cut and grinding feed rate had the same neutral effect on the resultant grinding forces.

Symbols

Symbol	Unit	Description
a_e	mm	Depth of cut in the grinding process
a_{ed}	mm	Depth of cut in the dressing process
A		Constant of the grinding tool micro-topography
BHN	N/mm^2	Brittle hardness
C	mm^{-2}	Density of the active grains
C_d	mm^{-2}	Dynamic cutting-edge density
C_s	mm^{-1}	Static cutting-edge density
$C_{d(z)}$	mm^{-2}	Dynamic cutting-edge density in the depth z into the grinding tool
$C_{s(z)}$	mm^{-2}	Static cutting-edge density in radial distance z into the grinding tool
D	mm	Diameter of indenter in Brinell hardness test
d	mm	Impression diameter in Brinell hardness test
d_f		Empirical factor
d_e	mm	Equivalent grinding tool diameter
D_{tip}	mm	Cutting edge diameter
E_s	N/mm^2	Modulus elasticity of the grinding tool

(continued on next column)

(continued)

Symbol	Unit	Description
E_w	N/mm^2	Modulus elasticity of the workpiece
F_t	N	Tangential force
F_n	N	Normal force
F'_t	N/mm	Specific tangential force
F'_n	N/mm	Specific normal force
F''	N	The resultant force per active grain
F''_t	N	Tangential force per active grain
F''_n	N	Normal force per active grain
h	mm	Depth of indentation in Brinell hardness test
h_{cu}	μm	Undeformed chip thickness
h_{cu-max}	μm	Maximum undeformed chip thickness
h_{cr}	μm	Critical chip thickness
K		Constant of the wheel topography
K_s	mm^2/N	Grinding tool elasticity
K_w	mm^2/N	Workpiece elasticity
l_c	mm	Contact length between the grinding tool and material
N_d		Number of active grains in the material-tool contact zone

(continued on next page)

(continued)

q_d		Dressing speed ratio
R_r		Constants which represents the roughness of the contact surface
U_d		Dressing overlap ratio
v_w	mm/min	Feed rate
v_w/a_e	mm/mm.min	Feed-rate-to-depth-of-cut ratio
v_c	m/s	Cutting speed
v_{ftd}	mm/min	Dressing feed rate
V_{valley}	mm³	The volume of the shadow behind the active cutting edges
V_{tot}	mm³	The total volume of the tool engaged with the workpiece
V''_{valley}	mm³	The volume of the shadow generated by each single active cutting-edge
w material	mm	Width of contact between the grinding wheel and
z	μm	Radial distance into the grinding wheel
ε	degree	Infeed angle
δ function	μm	Mode value in Rayleigh probability distribution
ρ		Empirical factor
μ		Friction coefficient

1. Introduction

In many industrial sectors the demands for manufacturing precise micro-parts with a high level of accuracy and complexity is increasing. These micro-parts are generally complex and have strict requirements, such as high accuracy, and surface integrity. Finding a manufacturing process that could provide a high level of accuracy and guaranty the part quality with complex features is challenging. A robust manufacturing process to fulfill such stringent requirements is mechanical micro-machining. Among mechanical micro-machining, micro-grinding offers several advantages such as flexibility, higher quality and workpiece material independency in the fabrication of micro-scale parts and features over other mechanical micro-machining processes. Contrary to the conventional (macro) grinding process, which is typically employed for grinding of simple components, the micro-grinding offers a high degree of geometric flexibility to produce micro-parts with sophisticated features. Some examples are micro-sensors, micro-actuators, micro-fluidic devices, and micro-machine parts. Its further distinction to conventional grinding includes inherent tool deflection and the size effect associated with very small chip thicknesses (e.g. 0.4 μm) [1–3].

The research on micro-grinding process is mostly related to the grindability studies. Zhang et al. [4] investigated the surface generation mechanism in micro-grinding of RB-sic/Si composites. They showed that the surface roughness could be modeled via the micro-pits' distribution, corresponding to the random and stochastic properties of the diamond grits as well as the micro-pits formation during the material removal process. Zhou et al. [5] studied the effect of process parameters on the quality of the finished surface and subsurface recrystallization of nickel-based (single-crystal) super-alloys. They concluded that decreasing the cutting speed and increasing the feed rate, the depth of cut worsened the surface quality. The tool wear monitoring during ceramic micro-grinding was examined by Feng et al. [6,7]. They demonstrated that the tool wear could be monitored without any characteristics machining knowledge and presented a model to predict the ground surface quality. Ho Lee and Won Lee [8] investigated the performance of the micro-grinding process under compressed cold air. They showed that utilizing compressed cold air is a useful method for reducing forces when a low depth-of-cut and a low feed rate are employed. They stated that the technique is more effective for electroplated instead of vitrified cBN tools. Smith et al. [9] developed a robust diamond micro-grinding tool that produced superior ground surface and showed better tool life compared to conventional, electroplated diamond micro-grinding tools.

Although there are some similarities between the micro and conventional grinding process, the micro-grinding process is distinctive because of the size effect. Therefore, the outputs of micro-grinding like the surface quality and micro-grinding forces are related to the mechanical and thermal interactions between a single grit and the work material. Hence, an analytical description of the single grit-workpiece interaction is critical for better process understanding. This interaction can be defined by maximum undeformed chip thickness, the effect of plowing, and friction coefficient. Thus, the grinding process can be described via modeling of the chip thickness, which is governed by a multitude of parameters and factors. Since a grinding process involves material removal with a large number of abrasive grains (with geometrically undefined cutting edges) which are randomly districted over the surface of the grinding tool with different shapes and cutting edges, it is challenging to study and model the chip thickness and consequently material removal mechanisms. Nevertheless, this random distribution results in a probabilistic distribution of cutting edges – resulting in a random distribution of various chip thicknesses. Using the chip thickness prediction, modeling of the of grinding forces and surface roughness is achievable. This prediction can further assure the process control and optimization [10].

In view of this complexity, there are several ways to model the undeformed chip thickness and to describe grain-workpiece interactions in the grinding process. The undeformed chip thickness can be directly modeled via analyzing the grinding path or by quantifying the balance between the volume of the generated chips and the total material removal rate [11]. Yang et al. [12,13] modeled the chip thickness under different friction coefficient based on the strain gradient, and geometry and kinematics analyses. They showed that the chip thickness in grinding and single grain test of ceramic materials decreased with the increasing the friction coefficient and frictional angle. Moreover, they addressed the size effect in their study and concluded that the critical chip thickness is in the border area of ploughing, cutting, and mainly in the ploughing region. Agarwal and Rao [14] developed a new undeformed chip-thickness model for grinding of ceramics. This model considers the stochastic nature of the grinding process, i.e. the random geometry and the random distribution of cutting edges. Zhang et al. [15] modeled a wheel topography with the integration ability with the workpiece model, kinematic model, and undeformed chip thickness model. The proposed tool topography model, aided by a single grain model, could calculate the distribution of undeformed chip thicknesses. In most of the studies, the deformation of the grinding contact zone is not considered. Moreover, none of these analyses take the dressing parameters explicitly into the account. Varying the dressing parameters can significantly change the number of active cutting edges in the tool-workpiece contact zone, which affects the undeformed chip thickness.

Since the research in the field of micro-grinding is still in its early stage, there are not many modeling-focused studies available. Cheng et al. [16] built a micro-fracture model and established a restraining technique for micro-grinding of glass and also proposed a prediction model for the size of the fractures considering both micro-interaction and elastic strain energy. With the help of the model, they could increase the productivity of the process up to 50 times. Cheng and Gong [17] modeled the process forces considering crystallographic effects in micro-grinding of single-crystal silicon. They used the undeformed chip thickness to connect the process parameters and grinding forces. They found a critical chip thickness that determines a threshold for material-removal effectiveness. Kadivar et al. [18] modeled the grinding forces and surface roughness using the experimentally determined (single-grain) forces and material pile-up as a function of the grain size, the cutting speed, and the depth of cut. They extended the results of a single-grain test further to the aggregate action of the cutting grains in a grinding process through the kinematics of the process. Li et al. [19] modeled the grinding forces in detail, including rubbing, plowing, and cutting forces. In their method, the instantaneous grain-workpiece interaction for each grain was determined. The instantaneous
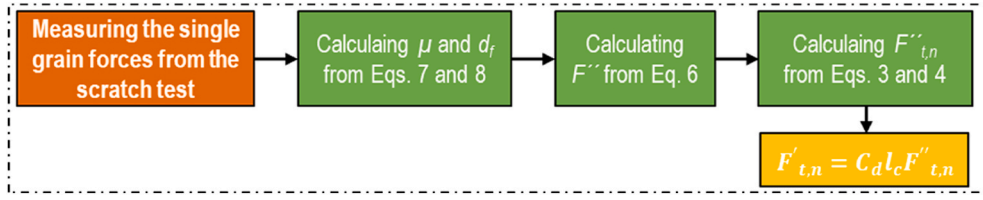
Fig. 1. The algorithm to the establishment of the force model.

interaction takes both random grinding-tool topography and process kinematics into consideration. Cheng et al. [20] presented a predictive model for the grinding force in micro-slot-grinding of single crystal sapphire. They concluded that the {0001} crystal orientation generated lower grinding forces compared to other directions. They also reported a force ratio between 0.6 and 0.8. They demonstrated that their prediction model could capture the main trend of the grinding forces. A thermo-physical model for micro-grinding was presented by Gorodkova et al. [21]. The model was able to predict the cutting zone temperature and the temperature distribution in the workpiece, considering the process parameters as well as the properties of the material.

One can observe that most available studies consider the probabilistic nature of the grinding process. However, the effects of tool deflection and dressing parameters are not considered in these models. Therefore, an attempt is made to develop a model to predicting cutting forces considering the effects of dressing parameters and tool deflection. In this approach, a probabilistic function of chip thickness, a chip thickness model based on the kinematics of the process, a topography of the tool, and material properties are considered. The micro-topography of the grinding tool is modeled as a function of dressing parameters. The local deflections of every single grain in the contact zone are also considered in the chip thickness model. First, the chip thickness is represented by the Rayleigh probability distribution function (p.d.f) relating the kinematic conditions, the real contact length, and the dynamic cutting edges density. In the second step, both the real contact length and the dynamic cutting-edge density were calculated through the dynamic effects of single grain forces. The chip thickness was then calculated iteratively, based on each incremental single grain force for a corresponding (instantaneous) chip thickness. The individual grain forces then integrated for the whole grinding tool using the dynamic cutting-edge density. In the next step, according to the actual depth of cut and the calculated grinding forces, the tool deflection was determined, and the depth of cut was corrected. Such modified depth of cut was then considered for more realistic calculation of grinding forces and chip thickness. The results show that the prediction model can precisely predict the tangential and normal grinding forces with a mean accuracy of 10% and 28%, respectively without considering the correction factor.

2. Modeling

2.1. Modeling of grinding forces

In the grinding process, the resultant forces for every single grain (the grain which comes in contact with the workpiece) can be aggregated to the whole grinding tool in order to model the grinding forces. Therefore, the tangential and normal grinding forces, $F''_{t,n}$, can be expressed as a function of single grain forces considering the dynamic cutting-edge density, C_d, and the real grinding tool-workpiece contact length, l_c, as the following:

$$F'_{t,n} = C_d l_c F''_{t,n} \tag{1}$$

According to Shaw [22], the indentation test can be used to define the single grain forces. To this end, the indentation force in Brinell hardness test can be combined with the single-grain test. The Brinell hardness equation is presented in Eq. (2):

$$BHN = \frac{2F''}{\pi D \left(D - \sqrt{D^2 - b^2} \right)} \tag{2}$$

The material used in this study has the Brinell hardness of 3.5×10^{-3} N/mm^2. In Eq. (2), the load in Brinell test is shown as F''. This load can be supposed to be the acting force on each abrasive grain in the grinding process. D is the indenter diameter (here the diameter of the diamond tool in the single scratch test which had pre-defined form with a spherical tip), and b defines the impression diameter.

In the grinding process, firstly the spherical grains (assumed in this study for calculating the single grain forces) indent the workpiece–generating some plastic deformation, like the Brinell hardness test. The abrasive grains then move in the horizontal direction. This horizontal movement pushes the plastically deformed zone in the front of abrasive grains and shears the material and produces chips – acting as an extrusion process [22]. This horizontal movement also generates a friction force between the abrasive grain and material as well as the generated chip. Therefore, the tangential and normal cutting forces can be calculated as a combination of the single grain force from the Brinell hardness test and friction coefficient, μ:

$$F''_t = F''(\sin(\alpha) + \mu \cdot \cos(\alpha)) \tag{3}$$

$$F''_n = F''(\cos(\alpha) + \mu \cdot \sin(\alpha)) \tag{4}$$

The effective attack angle, α, presents the angle between the resultant and normal force, and can be geometrically expressed from the kinematics of the single grain cutting process as the following:

$$\alpha = cos^{-1} \left(1 - \frac{2h}{D} \right) \tag{5}$$

Since the diameter of D is constant the angle of α can be changed with changing the penetration grain depth, h (the maximum chip thickness in every single scratch). The strain rate used in the Brinell hardness test is very low. Moreover, the abrasive grains in the real process are not perfectly sphered. Additionally, high temperatures in the cutting zone cause material softening and consequently lower cutting force needed for the grain indentation. Hence, to calculate F'' the empirical factor of d_f is added to Eq. (2). Therefore, the F'' can be calculated using the following equation:

$$F'' = d_f \frac{\pi \cdot D \cdot BHN}{2 \left(D - \sqrt{D^2 - (D \cdot \sin(\alpha))^2} \right)} \tag{6}$$

The friction coefficient, μ, and the empirical factor of d_f can be determined from the single grain test on titanium alloy. By substituting the tangential and normal forces obtained from the single grain in Eqs. (3)–(5), the friction coefficient and d_f can be expressed as:

$$\mu = \frac{\left(F''_t \cdot \cos(\alpha) - F''_n \cdot \sin(\alpha) \right)}{\left(F''_t \cdot \sin(\alpha) + F''_n \cdot \cos(\alpha) \right)} \tag{7}$$

$$d_f = \frac{2\sqrt{F''^2_t + F''^2_n}}{BHN \cdot \pi \cdot D \left(D - \sqrt{D^2 - b^2} \right)} \tag{8}$$

Fig. 1 shows the flowchart to calculate the grinding forces from the
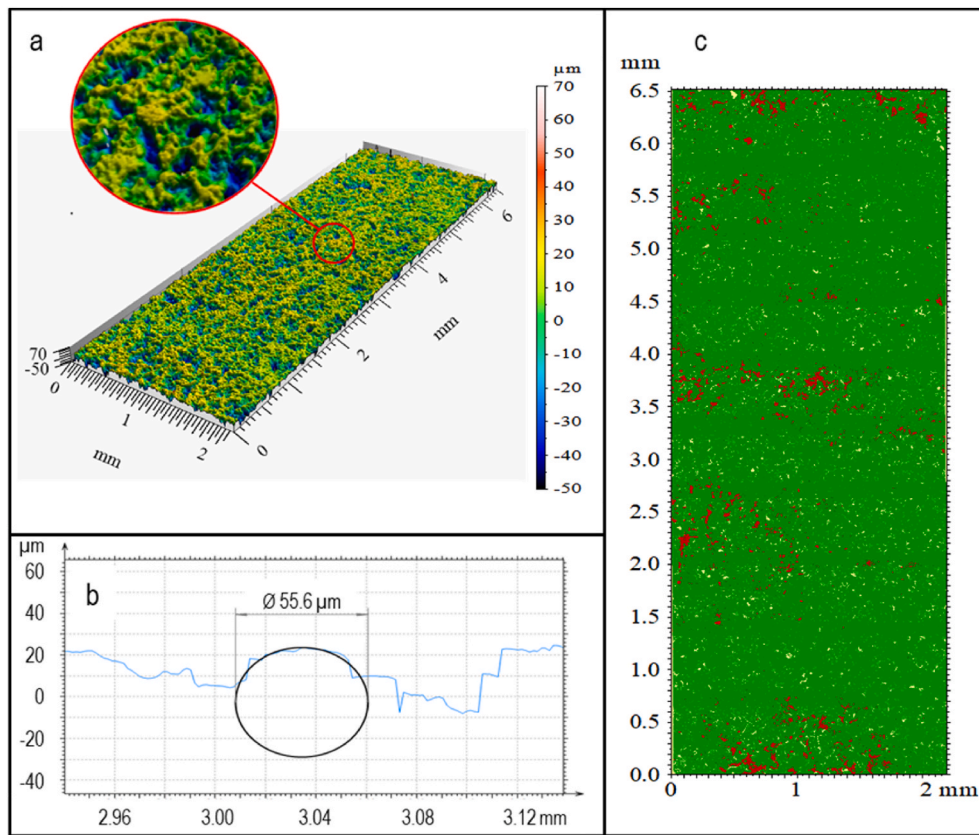
Fig. 2. a) a confocal microscopic picture from the grinding tool, b) the tip radius of a selected abrasive grain, c) the counted grain at a certain radial depth into the grinding tool.

scratch test. It is worth mentioning that the single grain test was done at the feed speed, v_w, of 5000 mm/min to prevent slots overlapping, different cutting depths, which represent different chip thicknesses in the micro-grinding process, and at the same cutting speed in which the grinding tests were carried out, i.e $v_c = 6, 10$ m/s.

2.2. Modeling of dressing process

The static number of the cutting edges quantifies the micro-topography of the grinding tool and changes with varying dressing parameters. In our previous work [2], it was reported that the dressing

parameters, such as the dressing overlap ratio and the dressing speed ratio have a significant influence on both grinding forces and surface roughness in micro-grinding of titanium. The tool topography and hence the number of static and dynamic cutting edges changes by varying these parameters. The consideration of dressing parameters in grinding force modeling is typically not explicitly considered. To model the grinding forces, the number of static cutting edges versus the radial position into the abrasive tool for different dressing parameters, i.e., dressing overlap ratio, U_d, and speed ratio, q_d, is considered here. The dressing overlap ratio defines the number of sequences that every peripheral line over the surface of the grinding tool comes into the contact
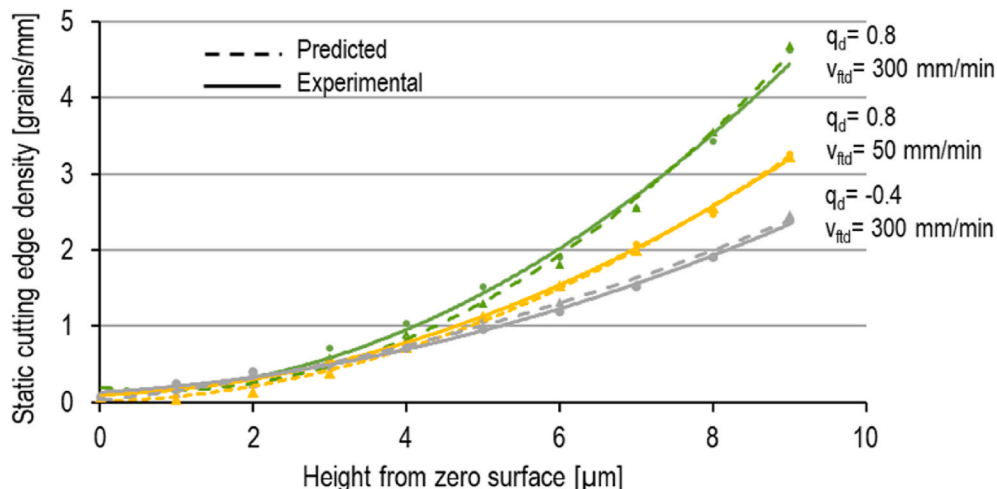
Fig. 3. Static cutting edge density versus the radial depth into the wheel.

with the dressing tool in the axial direction. The higher this value the higher the number of sequences and the lower the dressing feed rate. In rotary dressing, the dressing speed ratio is the ratio of the dresser cutting speed and the grinding tool. The dressing speed ratio can be categorized in up-dressing for the values lower than zero ($q_d < 0$) and down-dressing for the values higher than zero ($q_d > 0$) [2,23].

To this end, several grinding tools were dressed with various dressing parameters and for each grinding tool, the whole surface of the grinding tool was captured via a confocal microscope (Fig. 2a). From each picture, grain tip diameters (Fig. 2b) and the number of static grains (Fig. 2c) were counted and measured in different radial depths into the tool (z) from the highest point (zero point). The increment of 1 μm was chosen for the measurements. From the measurements, an average grain tip (cutting edge) diameter was selected for the modeling which is used to calculate the conical angle of the abrasive grain. In Fig. 2c the red regions show the area of the material of the grinding tool in a certain radial position into the tool (z). These red regions can be either abrasive grains or bonding material. The position of red points in Fig. 2c can be easily found in Fig. 2a. By focusing on the location, it can be realized whether it is an abrasive grain or bonding material. At each position, the tip diameter of every single grain was also measured, as shown in Fig. 2b.

A Gaussian Process Regression (GPR) was used to model the static number of the cutting edges. GPR is a non-parametric regression technique. In addition to predicting the response value for given predictor values, GPR models optionally return the standard deviation and prediction intervals. The method is effective even with a small number of experimental data and can provide estimates of uncertainties. Fig. 3 shows both predicted and real static cutting-edge density in different radial depths into the micro-grinding tool (z). The predicted values are in good agreement with the experiments. The GPR model could predict the static cutting-edges density with an average error of 10%.

2.3. Modeling of chip thickness

To determine the chip thickness in the micro-grinding process, first, the density of dynamic cutting edge, C_d, must be determined. C_d is a function of static cutting edges density, C_s, and process parameters i.e., cutting speed, depth of cut, and feed rate. Simultaneously, the C_d is also influenced by the cutting force acting on every single grain because of the tool deflection in the contact area. In the macro-grinding process, the static cutting-edge density exponentially increases by moving radially into the grinding wheel (z), and can be defined as follows [11,24–26]:

$$C_{s(z)} = Az^k \tag{9}$$

But the static cutting-edge density measured in the micro-grinding tool showed that the above equation is not valid, and the static cutting edges density changes according to Eq. (10) with the radial position into the tool (z). Therefore, the following equation was chosen for the simulation of the micro-grinding process:

$$C_{s(z)} = Ae^{kz} \tag{10}$$

where A and k are constants, and z is the radial distance into the tool. To obtain the A and k constants, firstly the static cutting-edge density at different z and dressing parameters was modeled using GPR model. Then, Eq. (10) was fit to the modeled static cutting-edge densities and the constants were defined for each different dressing parameter set.

The dynamic cutting-edge density, $C_{d(z)}$, is a function of static cutting-edge density and process kinematics. The dynamic cutting-edge density is lower than the $C_{s(z)}$. In the grinding process after each abrasive grain-workpiece engagement, a slot is cut and a 3D space including valleys (voids) and pile-ups are left along its moving path. Then the next grain comes into the contact with the workpiece. The new grain either remove some material along its moving path or traverses between the valleys (voids) generated by the previous grains. It highly depends on

the protrusion height and position of each grain on the grinding tool surface. In fact, all the static cutting grains do not contribute to the cutting process but some of them. Hence, the number of dynamic cutting-edges is always lower than the static numbers. Therefore the $C_{d(z)}$ can be defined geometrically as:

$$C_{d(z)} = C_{s(z)}\left(1 - \frac{V_{valley}}{V_{tot}}\right) \tag{11}$$

In Eq. (11) V_{valley} is the volume of the valleys (voids) left behind the active cutting edges defined in Eq. (12), and V_{tot} defines the total volume of the grain-workpiece engagement given in Eq. (13) [26]:

$$V_{valley} = N_d \cdot V'_{valley} \tag{12}$$

$$V_{tot} = l_c \cdot w \cdot z \tag{13}$$

where l_c shows the contact length and w is related to the width of cut, N_d represents the number of active grains in the contact zone, and V'_{valley} defines the volume of the valleys generated by each single active cutting-edge which is the integration of the cross-section area of the cut material, $A_{valley(x)}$, along the length of the groove, x [26].:

$$V'_{valley} = \int_0^x A_{valley(x)}dx \tag{14}$$

It is worth mentioning that the spherical shape of grain is used in the single grain force modeling recommended by Shaw [22]. However, to analyze the grain-workpiece interaction, conical shape is used for modeling because of the mathematical simplifications. In the grinding process, the relative movement of the abrasive grain generates a curved longitudinal chip. This chip has a thickness starting from zero to its maximum value known as the maximum chip thickness, h_{cu-max}. In this study, to simplify the chip thickness model, an idealized long slab chip with a triangular cross-section was assumed. This chip has a uniform thickness and width of h and b, respectively. Hereafter the parameter h is representing the maximum chip thickness. Assuming the abrasive grains with a conical form with the angle of 2θ in the grinding process $A_{valley(x)}$ can be written as:

$$A_{valley(x)} = h_x^2 \cdot (\tan\theta) \tag{15}$$

in which h_x expresses the chip thickness at the axial position of x and can be written as:

$$h_x = x \cdot \tan\varepsilon \tag{16}$$

By having the infeed angle of ε [25] as: $2\frac{v_w}{v_c}\sqrt{\frac{a_e}{d_e}}$, the V'_{valley} can be rewritten as:

$$V'_{valley} = h^3 \cdot \frac{\tan\theta}{3\tan\varepsilon} \tag{17}$$

The grinding tool consists of several abrasive grains which are stochastically distributed over the surface of the grinding tool. Hence, the chip thickness as a function of the tool topography can be determined via probability approaches. Younis and Alawi [27] used the Rayleigh p. d.f. for random distribution of the cutting edges in the grinding process as:

$$\begin{cases} f(x,\delta) = \frac{x}{\delta^2}e^{\left(\frac{-x^2}{(2\delta^2)}\right)} & x \geq 0 \\ o & x < 0 \end{cases} \tag{18}$$

In the Rayleigh function δ indicates scale parameter of the distribution in x which can be expressed as:

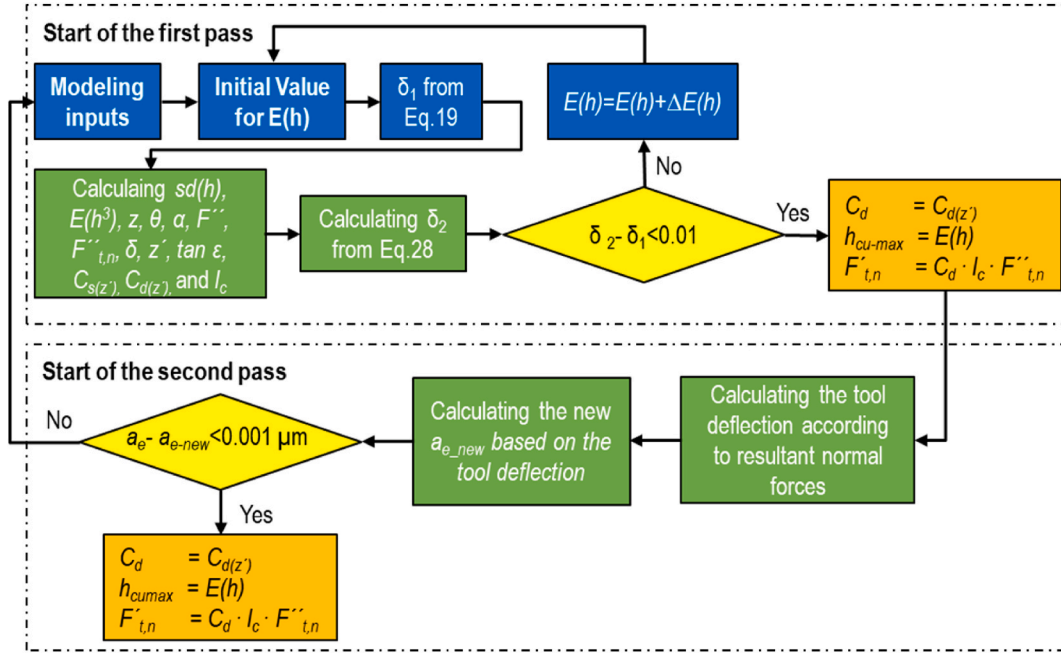$$E(x) = \sqrt{\frac{\pi}{2}}\delta \tag{19}$$

Fig. 4. Computational algorithm to predict grinding forces and tool deflection.

To apply this function to the modeling of grinding tool and chip thickness, the value of x can be replaced by the undeformed chip thickness h in grinding. The undeformed chip thickness is the engagement depth of each abrasive grain irrespective of the plowing and/or cutting material. Therefore, Eq. (17) can be written as:

$$V'_{valley} = \frac{\tan \theta}{3 \tan \varepsilon} E(h^3) \quad (20)$$

where $E(h^3)$ is:

$$E(h^3) = \int_o^\infty h^3 f(h) d(h) \quad (21)$$

By replacing $f(h)$ with the p.d.f in Eq. (21) we get:

$$E(h^3) = \int_o^\infty \frac{h^4}{\delta^2} e^{\left(\frac{-h^2}{(2\delta^2)}\right)} d(h) = 3.76 \ \delta^3 \quad (22)$$

The number of active grains, N_d, in the tool-workpiece contact zone can be calculated as:

$$N_d = l_c \cdot w \cdot C_{d(z)} \quad (23)$$

Therefore, Eq. (13) can be expressed as:

$$V_{sh} = l_c \cdot w \cdot C_{d(z)} \cdot \left(\frac{\tan \theta}{3 \tan \varepsilon}\right) 3.76 \delta^3 \quad (24)$$

and from Eq. (11), $C_{d(z)}$ can be stated as [26]:

$$C_{d(z)} = \frac{C_{s(z)}}{1 + \frac{C_{s(z)} \cdot \tan \theta \cdot E(h^3)}{3 \tan(\varepsilon) \cdot z}} \quad (25)$$

where, the variance, $sd(h)$, of the Rayleigh p.d.f is:

$$sd(h) = \left(\frac{4 - \pi}{2}\right) \cdot \delta \cdot = \cdot 0.655 \cdot \delta \quad (26)$$

The chip thickness is related to the kinematics of the process including the main process variables which can be found as follow:

$$h = \frac{aV_w}{V_c} \frac{1}{l_c C_d} \frac{1}{\tan \theta} \quad (27)$$

To define the distribution of the chip thickness, just those depths of engagements (chip thicknesses) must be considered which contribute to the material removal ($h > h_{cr}$). Thus, from the kinematics of the process, and assuming the chip with a triangular cross-section, Hecker et al. [26] defined the Rayleigh parameter of δ for the chip thickness as:

$$\delta = \sqrt{\frac{aV_w}{2V_c} \frac{1}{l_c C_d} \frac{1}{\tan \theta} - \frac{h_{cr}^2}{2}} \quad (28)$$

where h_{cr} is the critical chip thickness obtained from the single grain test which is 0.4 μm for Ti6Al4V and θ expresses the conical angle of the grain, which changes with varying the diameter of grains tip (here the average of grain's tip diameter), defined as:

$$\theta = 180 - \cos^{-1}\left(1 - \frac{2h}{D_{tip}}\right) \quad (29)$$

Using the parameter δ in Eq. (28) and replacing it in Eqs. (19 and 23) the expected chip thickness, h, and its standard deviation can be respectively calculated. The parameters of l_c, h and C_d are simultaneously updated and recalculated. The real tool-workpiece contact length, l_c, can be calculated using the following equation [25]:

$$l_c = \left(a_e \cdot d_e + 8R_r^2 \cdot F_n' \cdot d_e (K_s + K_w)\right)^{0.5} \quad (30)$$

The actual radial position into the grinding tool, z, which participates in the cutting is equal to the maximum chip thickness, thus:

$$z = \ E(h) + 3 \ sd(h) \quad (31)$$

R_r is a surface roughness constant in the contact zone which is taken to be equal to 5 in this study [22], d_e indicates the tool diameter, a_e shows the depth of cut, and K_s and K_w are tool and workpieces elasticity and can be defined as the followings:

$$K_s = \frac{1 - v_s^2}{\pi \cdot E_s} \quad (32)$$
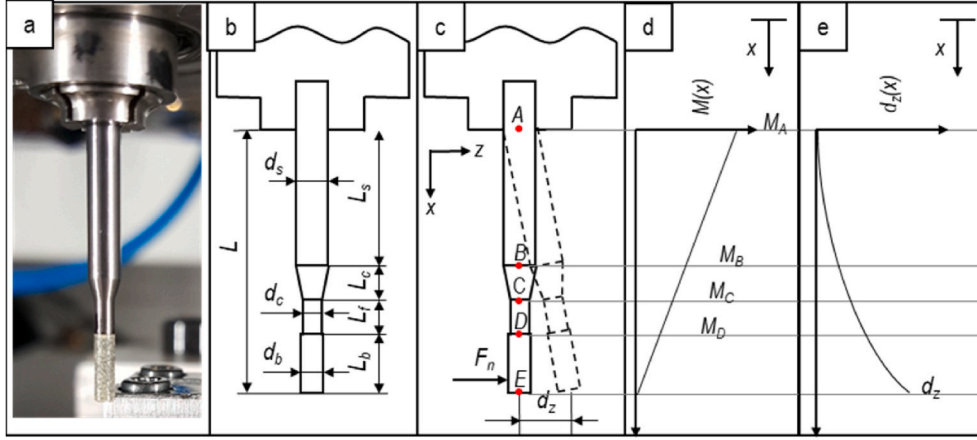
Fig. 5. Tool deflection model of micro-grinding tool a) micro-grinding tool, b) schematic of micro-grinding tool specification, c) schematic of micro-grinding tool deflection, d) Bending moment diagram, e) Deflection diagram.

$$K_w = \frac{1 - v_w^2}{\pi \cdot E_w} \tag{33}$$

E_s (37 × 10³ N/mm² [28,29]) and E_w (104 × 10³ N/mm²) are the elasticity modulus of diamond vitrified bonded grinding tool and Ti6Al4V workpiece, respectively. $v_s = 0.22$ ([28,29]) and $v_w = 0.33$ indicate the Poisson's ratios of the micro-grinding tool and workpiece, respectively.

The dynamic cutting-edge density depending on the chip thickness and tool-workpiece contact zone can be calculated using the above equations. To solve the equations, first, an initial chip thickness value (0.1 μm) was assumed for the p.d.f to predict the chip thickness using the C_d function. By means of a loop function, the chip thickness was changed incrementally to modify the value of chip thickness and C_d using Matlab. After the loop was successfully finished by calculating the C_d, l_c, and calculated forces for each single grain, the specific tangential (F'_t) and normal (F'_n) micro-grinding forces for the whole grinding tool were calculated (Eq. (1)).

After calculating the forces based on the actual depth of cut, the tool deflection was predicted and correspondingly, the depth of cut was corrected. The modified depth of cut was returned to the close loop and the new chip thickness and corresponding specific grinding forces based on the deflection of the grinding tool were calculated. The flowchart in Fig. 4 shows the modeling algorithm.

2.4. Modeling of tool deflection

The micro-grinding tool acts as a cantilever beam where the end of the tool is firmly clamped in the tool holder. The tool is subjected to a nonuniform cutting load at the end of the tool during the grinding process. Since the grinding forces are applied in two different directions (tangential and normal), the tool deflects in both directions. However, only the deflections in normal direction were considered in this study, since the tool is fed in the normal direction. The tool shaft was made of solid carbide with the E-Modulus of 6 × 10⁶ N/mm² and consisted of different sections with different geometries. To calculate the tool deflection accurately, the tool was divided into different geometrical segments, including the cylindrical section of the shaft, the taper, the free length, and the abrasive layer. The specific normal force applies to the abrasive layer. These sections, along with the actual micro-grinding tool, and the resultant deflection are shown in Fig. 5.

The total tool deflection, including the partial deflections of all sections, can be calculated using Euler–Bernoulli's beam theory. It is assumed that a concentrated force is applied to the middle of the grinding width a_p, which is the normal force (F_n) calculated from the first grinding pass with the actual depth of cut. The schematic of tool

deflection in each particular section of the tool (*A-E* in Fig. 3-c) is shown in Fig. 5d. The tool deflection of d_z at point *E* (Fig. 5e) is the total deflection of the tool as a result of F_n in Fig. 5c that can be expressed as the summation of deflections in points *A-D*. According to the Euler–Bernoulli's beam theory, the relationship between the tool's deflection and the applied load can be expressed as:

$$\frac{d^2z}{d^2x} = \frac{M(x)}{EI} \tag{34}$$

Since *EI* is a constant when double integrated and considering the boundary conditions of the tool (zero deflection and slope at point *A*), the tool deflection can be written as:

$$d_z = \frac{F_n L^3}{3EI} \tag{35}$$

Since the tool has multi sections, the tool deflection at point *E* can be written as the deflection of the tool at each point plus the accumulated slope at the specific point multiplied by the length of the section. Therefore, the tool deflection at point *E* can be expressed as:

$$d_z = \frac{F_n L_s^3}{3EI_s} + \left(\frac{F_n L_c^3}{3EI_c} + \frac{F_n L_s^2}{2EI_s} \cdot L_c \right) + \left(\frac{F_n L_f^3}{3EI_f} + \left(\frac{F_n L_s^2}{2EI_s} + \frac{F_n L_c^2}{2EI_c} \right) \cdot L_f \right)$$

$$+ \left(\frac{F_n L_b^3}{3EI_b} + \left(\frac{F_n L_s^2}{2EI_s} + \frac{F_n L_c^2}{2EI_c} + \frac{F_n L_f^2}{2EI_f} \right) \cdot L_b \right) \tag{36}$$

where $I_{s,c,c,b}$ are the area moments of inertia of the tool's cross-sections.

3. Experimental procedure

To validate the model, a series of trials were carried out on a high precision micro-grinding machine Kern Pyramid-Nano. The Ti6Al4V material in a block form was used for the experiments. Ti6Al4V has remarkable properties and is a suitable choice in many micro-manufacturing fields such as biomedical, healthcare goods, micro-fluidic, microneedles, and aerospace [30]. However, the machinability of this material is accompanied by high grinding forces, high tool wear, and burr formation – challenging the fabricating of high precision micro-parts. A diamond vitrified grinding tool with a diameter of 2 mm, grain size of 45 μm, and a concentration of 150 from Meister Abrasives AG was used. The tool was dressed with a rotary dresser roll from Dr. Keiser prior to each grinding test. The depth of dressing, a_{ed}, was set to 2 μm. Three sets of dressing parameters (sharp, medium, and timid), including different dressing speed ratios, q_d, and dressing overlap ratios, U_d, were used to test the dependency of the model on the dressing parameters. The micro-grinding forces were measured using a Kistler
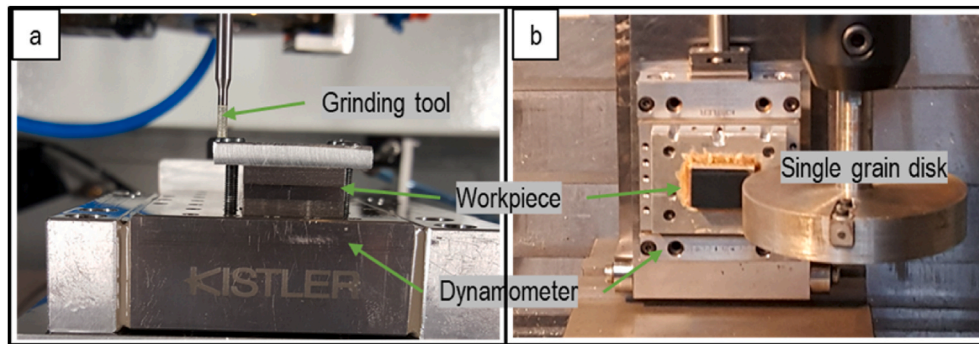
Fig. 6. The experimental setup for a) the micro-grinding test, b) the single grain test.

Table 1
Micro-grinding parameters.

Parameters	Values
Micro-grinding tool	D45-46-V-150
Workpiece	Titanium grade 5 (Ti6Al4V)
Cutting speed (v_c)	6, 10, and 14 m/s
Feed rate to depth of cut ratio (v_w/a_e)	5, 8, and 11 (x10^4 mm/mm.min)
Axial depth of cut (a_p)	3.5 mm
Coolant	Grinding oil (Oelheld SintoGrind OH 50071)
Dressing feed rate (v_{ftd})	50 and 300 mm/min
Dressing speed ratio (q_d)	−0.4 and 0.8
Dressing depth of cut (a_{ed})	3 × 2 µm

dynamometer type 9256C2. The experimental setup for the single grain test as well as the grinding test is shown in Fig. 6. The process parameters are listed in Table 1. The micro-topography of the grinding tool after each dressing set was captured using a µ-surf confocal microscope.

4. Results and discussion

4.1. Tool deflection

To find the contact between tool and workpiece, first, the zero point on the surface was set via an accurate contact measurement device integrated into the machine tool. Then, with 10 µm distance from the workpiece surface, the tool started to find contact with the workpiece with an increment of 1 µm until the acoustic emission sensor detected a contact. This point was set as a zero point. Three points on the workpiece surface (at the beginning, in the middle, and at the end of the grinding path) were measured via the taster and the coordinates of these three points were recorded. After grinding, these points were measured again, and the coordinates were recorded. The differences between the coordinates in each position from the programmed depth of cut were calculated and the mean value was chosen as the tool deflection in the micro-grinding process. The results of measured and calculated tool deflection are presented in Fig. 7. The maximum chip thickness was calculated from the model explained in the previous section.

From Fig. 7, it is clear that the grinding tool was subjected to a great tool deflection, especially when using aggressive grinding cuts associated with large chip thicknesses. This tool deflection is much higher than the actual depth of cut (the removed material from the workpiece). For instance, at the chip thickness of 1.4 µm, 33 µm depth of cut led to 8 µm removed material and 24 µm tool deflection. Therefore, to obtain an accurate force prediction, calculating the tool deflection plays a critical role. The more precise the tool deflection prediction, the higher the accuracy of the force modeling. The chip thickness in grinding is highly
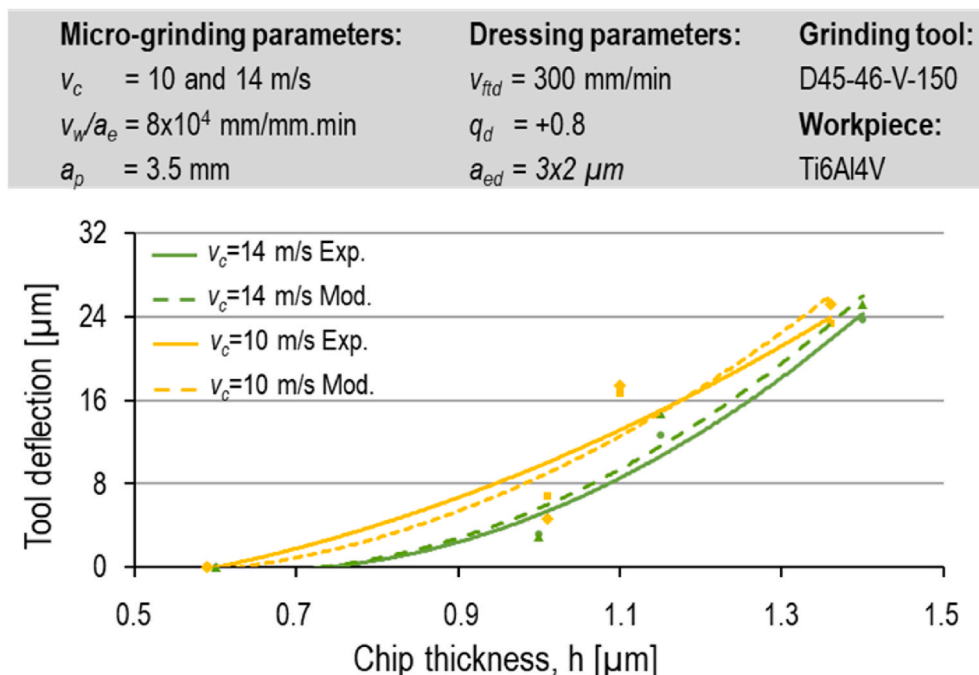

Fig. 7. The experimental and simulated tool deflection versus the chip thickness.
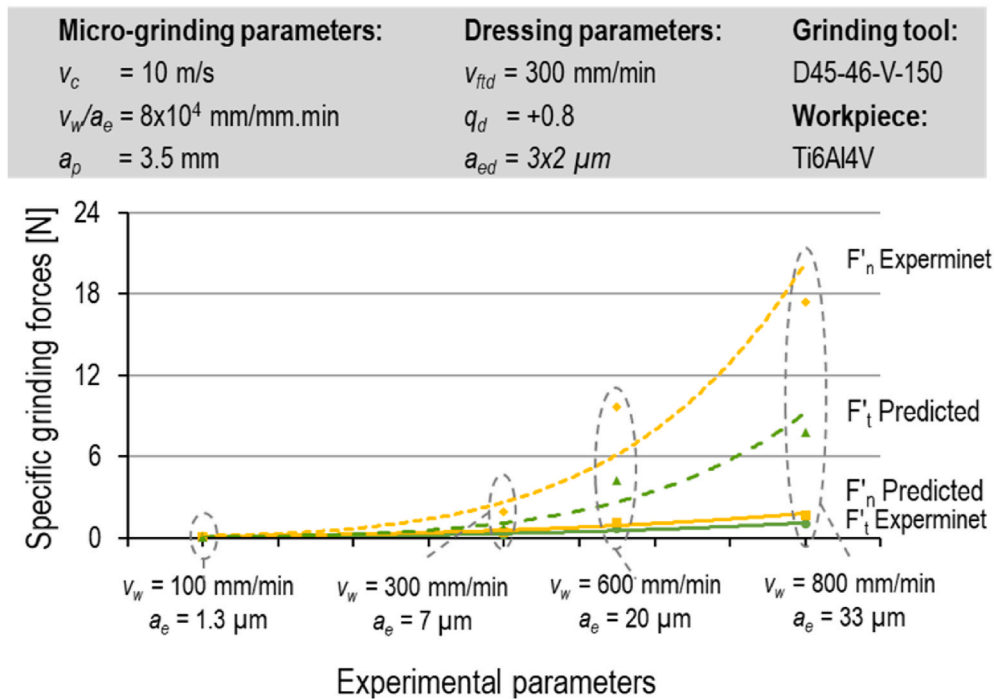
Fig. 8. The experimental and simulated grinding forces without consideration of tool deflection.
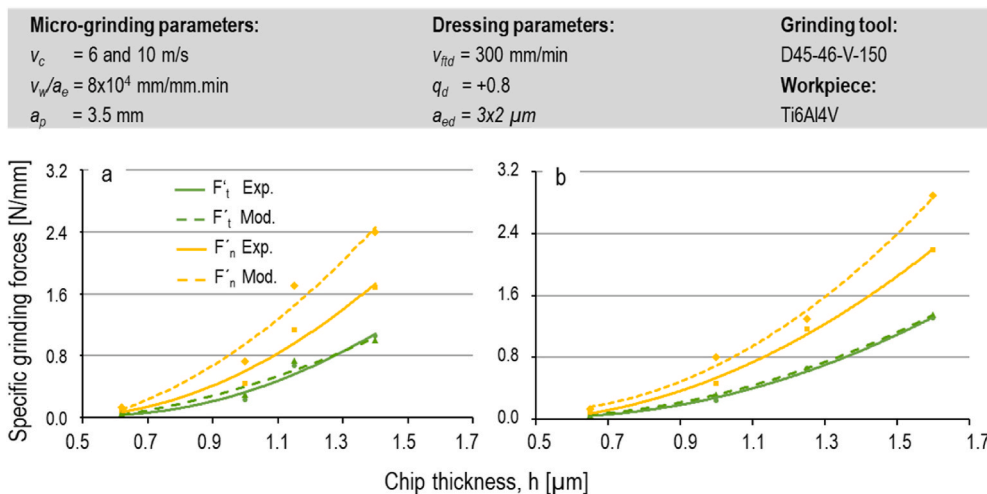

Fig. 9. The effect of chip thickness on specific grinding forces a) cutting speed 10 m/s ($a_{e\text{-real}}$ ranging from 1.3 to 9.2 µm and v_w varying between 100 and 800 mm/min), b) cutting speed 6 m/s ($a_{e\text{-real}}$ ranging from 1 to 7.6 µm and v_w varying between 77 and 620 mm/min).
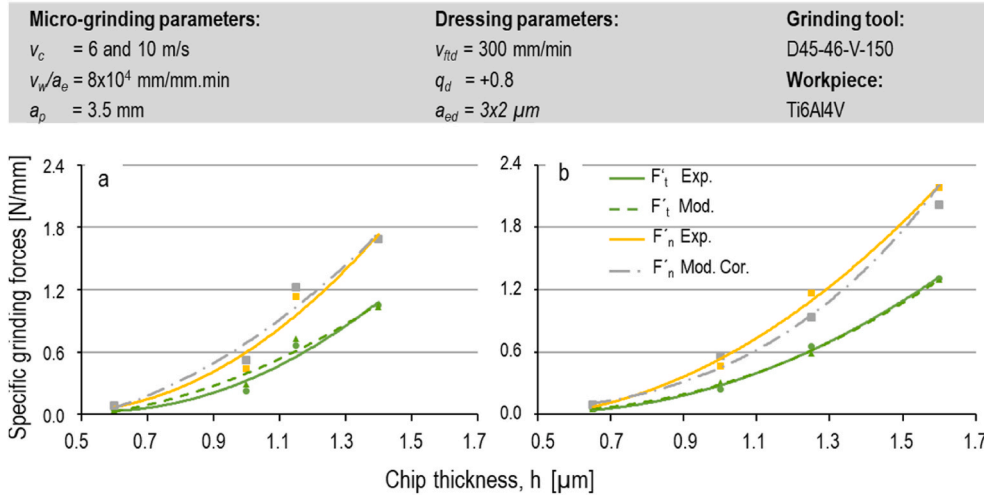
influenced by the grinding parameters. i.e., cutting speed, depth of cut, and feed rate. Since, in the theory and practice, the actual and theoretical cutting speeds and feed rates are the same, the chip thickness is greatly influenced by the real depth of cut. The model was capable of predicting the tool deflection with a mean error of 12% which shows the high reliability of the prediction model.

In order to show the relevancy of predicted forces to the tool deflection, the grinding forces were predicted first without considering the tool deflection and the results are presented in Fig. 8. The predicted grinding forces are in good accordance with the experimental results, where very fine grinding parameters are chosen ($v_w = 100$ mm/min and $a_e = 1.3$ µm) which induce almost no tool deflection. Micro-grinding the parts with more aggressive parameters resulted in tool deflection (Fig. 7). In this case the prediction model without considering the tool deflection gave rise to a great prediction error where the prediction

errors for the specific tangential and normal micro-grinding forces are 640 and 930% respectively for the test with $v_w = 800$ mm/min and $a_e = 33$ µm. Therefore, it is crucial to consider the tool deflection for predicting the cutting forces.

4.2. The effect of chip thickness

Fig. 9 shows the results of grinding forces from the modeling and experiments for different chip thicknesses. The specific tangential micro-grinding forces resulting from the model are in an excellent agreement with the experimental results (9% error for the tangential and 29% for the normal micro-grinding forces). This confirms the validity of the values considered for the friction coefficient (µ) and the empirical factor (d_f). Almost the same error for the modeling can be observed with increasing the chip thickness – showing the reliability of the model over

Micro-grinding parameters:	Dressing parameters:	Grinding tool:
v_c = 6 and 10 m/s	v_{ftd} = 300 mm/min	D45-46-V-150
v_w/a_e = 8x10^4 mm/mm.min	q_d = +0.8	**Workpiece:**
a_p = 3.5 mm	a_{ed} = 3x2 µm	Ti6Al4V

Fig. 10. The effect of chip thickness on specific grinding forces a) cutting speed 10 m/s (a_{e-real} ranging from 1.3 to 9.2 µm and v_w varying between 100 and 800 mm/min), b) cutting speed 6 m/s (a_{e-real} ranging from 1 to 7.6 µm and v_w varying between 77 and 620 mm/min).

a range of process operating conditions. However, the prediction of the specific normal forces shows a higher difference with the experiments, where the predicted values are always higher. This can be due to a number of assumptions used for the modeling purpose. The tangential grinding force is directly involved in the cutting process. The normal grinding forces are the resultant forces from the grain penetration into the workpiece. In this study, it is assumed that the cutting grains are idealized spheres, with an assigned average value for their size. However, in reality, each grain has its unique and random geometry and size. The real cutting grains are much sharper than the simulated ones. Therefore, they can penetrate the workpiece more efficiently – resulting in lower specific normal grinding forces. Moreover, the chip loading is not considered in the models, which can have a significant influence on normal forces. It is worth mentioning that both parameters µ and d_f were obtained from the single grain test. And their values change with varying the chip thickness. The results of single-grain test showed that the cutting speed has no influence on µ and d_f.

Fig. 9 reveals that the specific normal micro-grinding forces follow the same trend as the forces measured in experiments but with some systematic errors due to the assumptions mentioned above. Since the trend is the same an empirical factor, ρ, is defined to predict the normal grinding forces. Therefore, F'_n from Eq. (1) can be modified as:
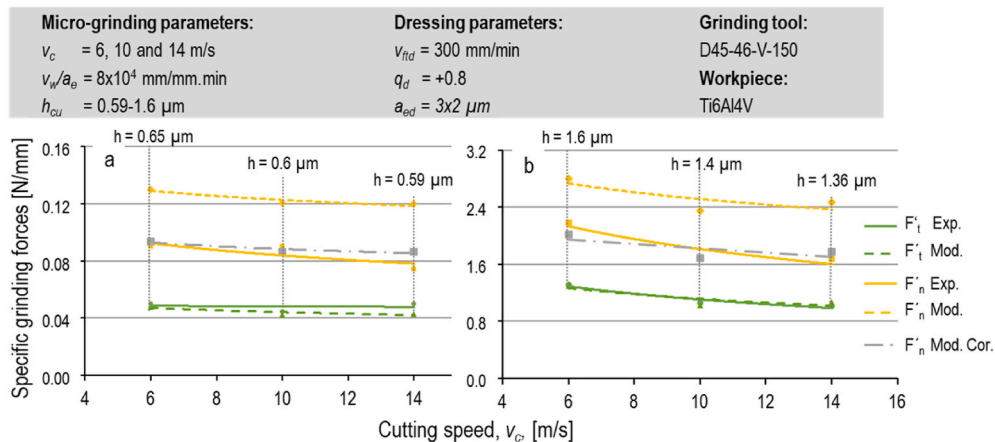
$$F'_n = \rho \cdot C_d \cdot l_c \cdot F''_n \qquad (37)$$

Based on Eq. (37), the normal grinding forces were calculated again, and the results are shown in Fig. 10. The prediction error for the specific normal grinding force (shown with discontinuous grey line) can be reduced to significantly (10%) by using the empirical factor.

4.3. The effect of cutting speed

In Figs. 9 and 10 the results of the modeled and experimental forces indicate that changing the cutting speed has minimal influence on the tangential grinding forces and the normal grinding forces reduced slightly at the same chip thickness. Changing the cutting speed varies the strain rate in the cutting process. Since the diameter of the grinding tool in the micro-grinding process is small (in this case, 2 mm) and the rotational speed in the machine tool is limited, changing the cutting speed in a large increment is not possible. The results imply that changing the cutting speed from 6 to 14 m/s has a minor effect on the flow stress of material in the cutting process. However, the strain rate became almost doubled.

Fig. 11 further clarifies the above-mentioned point. In this figure, the chip thicknesses for cutting speeds 10 and 14 m/s are 0.6 µm (Figs. 11a) and 1.4 µm (Fig. 11b), respectively, and 0.65 (Figs. 11a) and 1.6 µm (Fig. 11b) for the cutting speed of 6 m/s. These changes in the chip thickness are resulting from the prediction error of the tool deflection. At the cutting speed of 6 m/s, where the chip thickness is larger, higher

Micro-grinding parameters:	Dressing parameters:	Grinding tool:
v_c = 6, 10 and 14 m/s	v_{ftd} = 300 mm/min	D45-46-V-150
v_w/a_e = 8x10^4 mm/mm.min	q_d = +0.8	**Workpiece:**
h_{cu} = 0.59-1.6 µm	a_{ed} = 3x2 µm	Ti6Al4V

Fig. 11. The effect of cutting speed on specific grinding forces a) average chip thickness of 0.63 µm (a_e ranging from 1 to 1.5 µm and v_w varying between 77 and 119 mm/min), b) average chip thickness of 1.5 µm (a_e ranging from 7.6 to 11.7 µm and v_w varying between 347 and 800 mm/min).
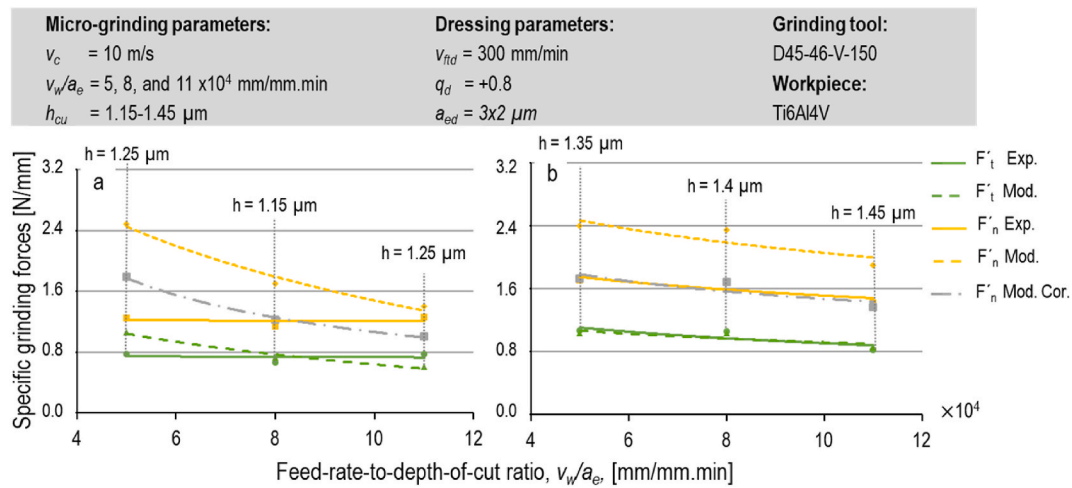
Fig. 12. The effect of feed-rate-to-depth-of-cut ratio on the specific grinding forces a) average chip thickness of 1.27 µm (a_{e-real} ranging from 6.6 to 9.1 µm and v_w varying between 474 and 705 mm/min), b) average chip thickness of 1.43 µm (a_{e-real} ranging from 8.1 to 13 µm and v_w varying between 633 and 940 mm/min).

tangential forces were observed (both modeled and experimentally obtained). Nevertheless, when changing the cutting speed from 10 to 14 m/s, where the chip thickness is similar, identical tangential grinding forces were generated. However, changing the cutting speed at the same chip thickness reduced the specific normal grinding force. This means that higher cutting speeds ease the penetration of the tool/grain into the material. Additionally, higher cutting speed in micro-grinding results in higher tool vibration [2,18]. This additional vibration in the process may also help the grain penetration into the workpiece, which is not considered in the models and which can explain the larger difference observed between the modeled and experimental normal forces at higher cutting speeds. Based on the results, the model could accurately predict the tangential (with 9% error) and normal (8% error with the modification factor and 31% without the modification factor) micro-grinding forces with changing the cutting speed.

4.4. The effect of feed-rate-to-depth-of-cut ratio

The previous section demonstrated that the cutting speed has a minor influence on grinding forces when the chip thickness was kept constant. Nevertheless, it is also necessary to examine the effect of another two important grinding parameters i.e., the depth of cut and the feed rate. To investigate the impact of both parameters in the abrasive process, a feed-rate-to-depth-of-cut ratio, v_w/a_e, is employed. With the help of this ratio, the effect of both parameters on the cutting forces at a constant chip thickness or constant material removal rate can be studied at the same time. The effect of this parameter for two different chip thicknesses on the specific micro-grinding forces is shown in Fig. 12. The figure expresses that there is no considerable change in the grinding forces with changing the v_w/a_e ratio. It means that neither a higher depth of cut nor larger feed rate has an influence on the grinding forces. However, it is recommended to grind the micro-parts with higher v_w/a_e ratios to obtained a better surface quality [3]. The predicted forces are also in a good agreement with the experimentally-measured forces except at the chip thickness of 1.2 µm and v_w/a_e ratio of 5×10^4 mm/mm.min. The reason for this seems to be the predicted tool deflection, which at this point is lower than the actual deflections. Lower tool deflection means erroneous depth-of-cut correction; in this case, the depth of cut is larger than the real a_e – causing higher normal and tangential micro-grinding forces. It is important to mention here that in all figures, the actual depth of cut is considered. The model could accurately predict the tangential (with 12% error) and normal (13% error with the modification factor and 29% without the modification factor) micro-grinding forces with changing the
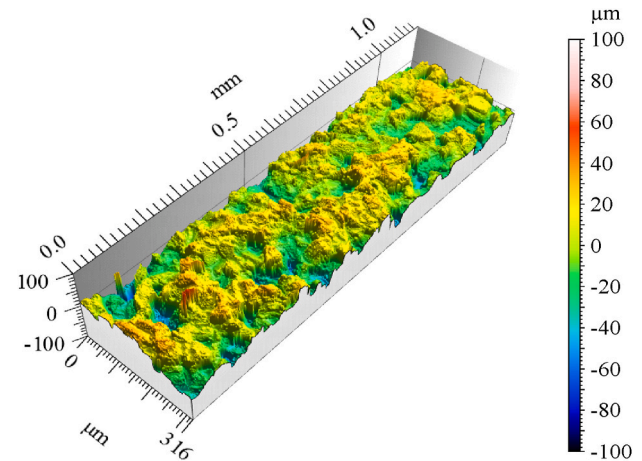
Fig. 13. The confocal picture from the micro-grinding tool after grinding with $v_c = 10$ m/s, $a_e = 6$ µm, $v_w = 480$ mm/min.

feed-rate-to-depth-of-cut ratio.

The micro-grinding tool was characterized after grinding in order to make sure that the tool was not subjected to sever wear which can affect the grinding forces. Therefore, a confocal microscope image was taken and presented in Fig. 13. It can be seen that the tool was not subjected to the grain flattening or grain pull-out, i.e. wear, and is in a good condition.

4.5. The effect of dressing parameters

To complete the analysis of the results it is necessary to investigate the influence of dressing parameters on the grinding process. The dressing parameters can substantially affect the grinding forces and the ground surface roughness [2,31–33]. As mentioned before, using different dressing parameters changes the micro-topography of the grinding tool, and consequently, the number of static grains (refer to Fig. 3). Parameters A and K (in Eq. (8)) for the estimation of the static grain density in a certain radial depth into the grinding tool are hitherto unknown. These two parameters change with different tool micro-topography as a result of varying dressing parameters. In the simulation model, the dressing parameters (like the grinding and material parameters) are given as inputs. By inputting the dressing parameters, the GPR model can predict the density of static grains in the radial depth into the tool. Here an exponential function (given in Eq. (8))
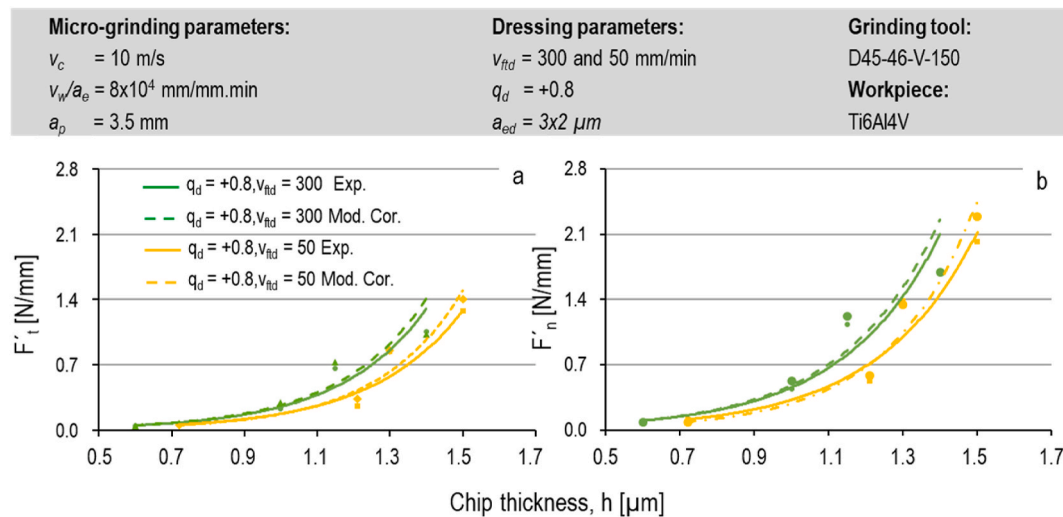
Micro-grinding parameters:	Dressing parameters:	Grinding tool:
v_c = 10 m/s	v_{ftd} = 300 and 50 mm/min	D45-46-V-150
v_w/a_e = 8x10⁴ mm/mm.min	q_d = +0.8	Workpiece:
a_p = 3.5 mm	a_{ed} = 3x2 μm	Ti6Al4V

Fig. 14. The effect of dressing parameters on the specific grinding forces a) tangential micro-grinding forces, b) normal micro-grinding forces.

was fit to the predicted grain densities and for each dressing parameter set; moreover, the parameters of A and K were experimentally determined and consequently, the grinding forces were predicted. The results in Fig. 14 show two different dressing parameter sets. According to the prediction results presented in the above figures, the empirical factor could precisely compensate the assumptions' errors in the modeling – hence higher accuracy for the prediction of specific normal grinding forces was achieved (13% error instead of 30%)

For the dressing analysis, the dressing feed rate, v_{ftd}, was used instead of the dressing overlap ratio, U_d. In macro-grinding process, where the diameter of the tool is much bigger than in micro-grinding; the overlap ratio typically ranges between 2 and 8. In micro-dressing, however, the rotational speed of the micro-tool is extremely high (e.g., almost 100.000 RPM for achieving the cutting speed of 10 m/s with a tool diameter of 2 mm), therefore achieving conventional U_d values would require extremely high dressing feed rates which are not attainable. As a result, the parameter v_{ftd} was used in this study. In our previous study, the effect of dressing parameters on the micro-grinding of the titanium alloy was investigated and showed that using lower dressing feed resulted in higher grinding forces and better surface finish [2]. The same effect was observed when up-dressing instead of down-dressing. Similar results were obtained here (see Fig. 14). Using more timid dressing parameters generated a finer tool topography – resulting in higher specific grinding forces. Fig. 14 indicates that the prediction model can precisely map the effects of dressing parameters on the micro-topography of the tangential (with 11% error) and normal (with 10% error) micro-grinding tool. Both simulations and experiments, proved that finer dressing results in approximately 19% higher grinding forces.

5. Conclusions

This study employed a probabilistic modeling approach for the estimation of chip thickness and specific forces in micro-grinding of Ti6Al4V with a vitrified-diamond grinding tool. The developed model incorporates the effects of dressing parameters and tool deflection. The following specific conclusions are drawn from this research:

- The static tool-deflection model, used in this study, showed that it can predict the tool deflection resulting from the normal grinding forces with acceptable accuracy.
- The cumulative static cutting-edge density could be fitted with an exponential function and has higher accuracy in predicting grinding

forces compared to the function proposed by other researchers in the macro-grinding process.
- The prediction model could rather precisely estimate tangential micro-grinding forces (mean error of 10%). However, this error was higher in the case of specific normal forces (mean error of 30%) because of the simplification considered in the model. Adding an empirical constant for the prediction of the specific normal forces could increase the accuracy of the prediction model up to 87%.
- From the modeling and experimental results, it can be concluded that the flow stress of the titanium did not change with increasing the strain rate in the range of tested cutting speeds (6–14 m/s). Thus, at a constant chip thickness, the specific micro-grinding forces are almost similar for the utilized cutting speeds. Moreover, the feed rate and depth of cut have the same impact on the specific grinding forces where the grinding forces did not change with changing the feed-rate-to-depth-of-cut ratio.
- The effect of dressing parameters on force modeling showed that even at the same chip thickness, finer dressing parameters resulted in higher cutting forces and the prediction model could precisely map the dressing parameters on the grinding forces.

It is worth mentioning that the explained model can be performed for all kind of materials since it is not using any material model but only the forces and friction and experimental coefficients from the single grain test. As the outlook of the work, the model will be validated for other kinds of materials to check the accuracy of the prediction model as well as the use of the empirical factor.

Declaration of competing interest

The authors declare that they have no known competing financial interests or personal relationships that could have appeared to influence the work reported in this paper.

Acknowledgment

References

[1] Kadivar M, Shamray S, Soltani B, Daneshi A, Azarhoushang B. Laser-assisted micro-grinding of Si3N4. Precis Eng 2019;60:394–404.

[2] Kadivar M, Azarhoushang B, Shamray S, Krajnik P. The effect of dressing parameters on micro-grinding of titanium alloy. Precis Eng 2018;51:176–85.

[3] Kadivar M, Azarhoushang B, Daneshi A, Krajnik P. Surface integrity in micro-grinding of Ti6Al4V considering the specific micro-grinding energy. Procedia CIRP 2020;87C:181–5.

[4] Zhang Q, To S, Zhao Q, Guo B. Amorphization and C segregation based surface generation of Reaction-Bonded SiC/Si composites under micro-grinding. Int J Mach Tool Manufact 2015;95:78–81.

[5] Zhou Y, Gong Y, Cai M, Zhu Z, Gao Q, Wen X. Study on surface quality and subsurface recrystallization of nickel-based single-crystal superalloy in micro-grinding. Int J Adv Manuf Technol 2017;90(5–8):1749–68.

[6] Feng J, Chen P, Ni J. Prediction of surface generation in microgrinding of ceramic materials by coupled trajectory and finite element analysis. Finite Elem Anal Des 2012;57:67–80.

[7] Feng J, Kim BS, Shih A, Ni J. Tool wear monitoring for micro-end grinding of ceramic materials. J Mater Process Technol 2009;209(11):5110–6.

[8] Lee P, Lee SW. Experimental characterization of micro-grinding process using compressed chilly air. Int J Mach Tool Manufact 2011;51(3):201–9.

[9] Butler-Smith PW, Axinte DA, Daine M. Solid diamond micro-grinding tools: from innovative design and fabrication to preliminary performance evaluation in Ti–6Al–4V. Int J Mach Tool Manufact 2012;59:55–64.

[10] Mirifar S, Kadivar M, Azarhoushang B. First steps through intelligent grinding using machine learning via integrated acoustic emission sensors. JMMP 2020;4(2):35.

[11] Malkin S. Grinding technology: theory and applications of machining with abrasives. Dearborn, Mich. op: Society of Manufacturing Engineers; 1989.

[12] Yang M, Li C, Zhang Y, Jia D, Li R, Hou Y, et al. Predictive model for minimum chip thickness and size effect in single diamond grain grinding of zirconia ceramics under different lubricating conditions. Ceram Int 2019;45(12):14908–20. https://doi.org/10.1016/j.ceramint.2019.04.226.

[13] Yang M, Li C, Zhang Y, Jia D, Li R, Hou Y, et al. Effect of friction coefficient on chip thickness models in ductile-regime grinding of zirconia ceramics. Int J Adv Manuf Technol 2019;102(5–8):2617–32. https://doi.org/10.1007/s00170-019-03367-0.

[14] Agarwal S, Venkateswara Rao P. Predictive modeling of undeformed chip thickness in ceramic grinding. Int J Mach Tool Manufact 2012;56:59–68.

[15] Zhang Y, Fang C, Huang G, Xu X. Modeling and simulation of the distribution of undeformed chip thicknesses in surface grinding. Int J Mach Tool Manufact 2018;127:14–27.

[16] Cheng J, Wang C, Wen X, Gong Y. Modeling and experimental study on micro-fracture behavior and restraining technology in micro-grinding of glass. Int J Mach Tool Manufact 2014;85:36–48.

[17] Cheng J, Gong YD. Experimental study of surface generation and force modeling in micro-grinding of single crystal silicon considering crystallographic effects. Int J Mach Tool Manufact 2014;77:1–15.

[18] Kadivar M, Zahedi A, Azarhoushang B, Krajnik P. Modelling of the micro-grinding process considering the grinding tool topography. Int J Autom Technol 2017;8(2):157.

[19] Li HN, Yu TB, Wang ZX, Zhu LD, Wang WS. Detailed modeling of cutting forces in grinding process considering variable stages of grain-workpiece micro interactions. Int J Mech Sci 2017;126:319–39.

[20] Cheng J, Wu J, Gong YD, Wen XL, Wen Q. Grinding forces in micro slot-grinding (MSG) of single crystal sapphire. Int J Mach Tool Manufact 2017;112:7–20.

[21] Gorodkova AE, Dyakonov AA, Herreinstein AV. Thermophysical modeling of microgrinding. Russ Eng Res 2017;37(7):647–50.

[22] Shaw MC. Principles of abrasive processing. Oxford University Press on Demand; 1996.

[23] Azarhoushang B, Kitzig-Frank H. Abricht-und schleiftechnologie 1-konditionieren von Schleifwerkzeugen-Abrichten, Profilieren und Schärfen 2019.

[24] Daneshi A. Micro chip formation mechanism in grinding of nickel-base superalloy-Inconel 718. University of Freiburg; 2019.

[25] Hecker RL, Liang SY, Wu XJ, Xia P, Jin DGW. Grinding force and power modeling based on chip thickness analysis. Int J Adv Manuf Technol 2007;33(5–6):449–59.

[26] Hecker RL, Ramoneda IM, Liang SY. Analysis of wheel topography and grit force for grinding process modeling. J Manuf Process 2003;5(1):13–23.

[27] Younis MA, Alawi H. Probabilistic analysis of the surface grinding process. Trans Can Soc Mech Eng 1984;8(4):208–13.

[28] Nakayama K, Brecker J, Shaw MC. Grinding wheel elasticity. Journal of Engineering for Industry 1971;93(2):609–13.

[29] Yamada T, Lee H. Study on elastic deformations of grinding wheels due to centrifugal forces. In: Proc. Of the ASPE. Annual Meeting; 2005; 2004.

[30] Kadivar M. Micro-grinding of titanium. Sweden): Chalmers Tekniska Hogskola; 2018.

[31] Linke B. Dressing process model for vitrified bonded grinding wheels. CIRP Annals 2008;57(1):345–8.

[32] Linke B, Klocke F. Temperatures and wear mechanisms in dressing of vitrified bonded grinding wheels. Int J Mach Tool Manufact 2010;50(6):552–8.

[33] Klocke F, Linke B. Mechanisms in the generation of grinding wheel topography by dressing. Prod Eng Res Dev 2008;2(2):157–63.